Characterization of Disruptions and Disruption-Related Effects for FIRE

(FIRE Disruption Design Description Document (DDD);
adapted from the ITER FDR Disruption DDD; changes/updates for FIRE in red text)

For FIRE vacuum vessel and in-vessel component design purposes, the most important disruption-related parameters are 1) the durations of the thermal and magnetic energy quenches and the partitioning of the corresponding plasma energies among the divertor and first wall (FW) surfaces and 2) the magnitude and toroidal asymmetry of the poloidal ('halo') current flow in conducting in-vessel structures that arises owing to rapid plasma vertical instability. The possibility of localized runaway deposition is also another important consideration for the design of at-risk plasma facing component (pfc) surfaces.

Table 1 summarizes the recommended physics design bases for these and related parameters in FIRE. The basis for this Table is a high-Q DT plasma, with initial current I_{p0} = 6.5 MA, as obtained at B = 10 T with q_{95} = 3.0. This plasma produces 200 MW fusion power at $\beta_N = \langle\beta\rangle aB/I \approx 2.5$: thermal and magnetic energies W_{th} and W_{mag} are respectively about 33 MJ and 35 MJ. Here W_{mag} includes the ex-plasma magnetic energy within the FIRE vacuum vessel. This vacuum vessel and the associate passive stabilizing structures, which have a toroidal resistance of ≈ TBD μΩ and an effective toroidal L/R time constant of ~60 ms, determine the passive stability of the plasma with respect to n = 0 modes (and hence the time-scale of VDE evolution) and also limit the in-vessel magnetic energy dissipation from the disruption or VDE current quench to ~W_{mag}.

The parameters given in Table 1 are generally the maximum or 'worst-case' limits expected. But as the Table makes clear, there are appreciable uncertainties in all of the FIRE disruption and disruption-related predictions, and so it will be prudent for vessel and in-vessel component designers to examine the consequences of the range of possible parameters. Specific discussion of the basis for each recommendation and of the associated uncertainties follows below. The presentation is organized into four Sections: 1) Thermal Quench, 2) Current Quench, 3) Runaway Electrons, 4) Vertical Instability and Halo Currents. Relevant data extracted from the *ITER-FDR Plasma Design Description Document (DDD)*, Chapter 6, and from Chapter 3, *MHD Stability, Operation Limits and Disruptions*, of the *ITER Physics Basis* is presented in these Sections. References as to the origin of the physics data cited are omitted herein, but can be found in the ITER DDD and the *Physics Basis*.

TABLE 1

FIRE Disruption and Disruption-Related Design Basis Recommendations

Parameter	Value (Range)	Comment
Frequency	10% (10-30%) per pulse	30% for plasma development ≤ 10% for mature (repetitive) operation
Number (3,000 full perform. attempts)	300 (900)	300 at full W_{th} and W_{mag}, balance at ≤ 0.5 W_{th} and full W_{mag}
Thermal energy	33 MJ	For typical 200 MW plasma
Thermal quench duration	0.2 (0.1–0.5) ms	Single or multi-step thermal quench, see text
Fraction of W_{th} to divertor	80–100%	By conduction to targets, up to 2:1 toroidal asymmetry, see text
Fraction of W_{th} to FW (baffle)	≤ 30%	By radiation (to FW) or conduction (to baffle)
In-divertor partition (inside/outside)	2:1 – 1:2	For SN plasmas. Significant uncertainty: see text. No data for DN plasmas
Poloidal localization in divertor	3-x normal SOL; (1-x to 10-x)	Incident energy, with up to 2:1 toroidal asymmetry. Plasma shielding and re-radiation will likely redistribute in-divertor energy
Magnetic energy	35 (?) MJ	For 6.5 MA, total out to VV
Current quench duration	6 (2-600) ms	Duration ≥30 ms: more-severe VDE and halo current
Maximum current decay rate	3 MA/ms	May occur only during fastest part of current quench; typical maximum rate ~1 MA/ms
Fraction of W_{mag} to FW, by radiation	80–100%	By radiation, with poloidal peaking factor ~ 2
Fraction of W_{mag} to FW, by localized conduction	0-20%	From VDE: depends on VDE evolution and in-vessel halo current. Hot-plasma VDEs may also deposit ~0.2-1.0W_{th} on localized portion(s) of FW. Toroidal alignment critical
VDE frequency	TBD (??? 1% of pulses, or 10% of disruptions???)	Presently very uncertain. May be able to maintain vertical position control after thermal quench. But margin/noise sensitivity is uncertain. Control failure will result in VDE or loss of after-thermal-quench control
Halo current fraction $I_{h,max}/I_{p0}$	0.4 (0.01-0.50)	Highest value may apply (depends on passive stabilizer configuration)
Toroidal peaking factor	2 (1.2 ≤ TPF ≤ 4)	TPF up to 2 yields ‘sinϕ’ distribution; TPF > 2 yields ‘localized filament’
$(I_{h,max}/I_{p0})$*TPF	≤ 0.50 (typical maximum)	Data bound is ≤ 0.75 (see text)
Runaway electron current (following disruption or fast shutdown)	50% I_p (0-50%)	Highly uncertain. I_{RA} > 1 MA requires ≥ 1 A seed source. Not expected in thermal plasma, but pellet shutdown may seed avalanche. MHD fluctuations may offset part or all of avalanche growth.
Runaway energy	~15 MeV	Limited by knock-on avalanche

Localization of runaway deposition	≤ 1 m^2	Poloidal localization to a ~0.1-m (poloidal) section of the FW or divertor target expected; toroidal localization depends on pfc and wall alignment to toroidal field

1. Thermal Quench Characteristics. Thermal quench duration is estimated to be 0.1-0.5 ms: the range reflects uncertainty in application of data to FIRE size (Fig. 1) and also the observation that thermal quenches are sometimes single-step and sometimes multi-step, wherein energy loss occurs in two or more rapid steps separated by a delay that extrapolates to ~1 ms for FIRE.

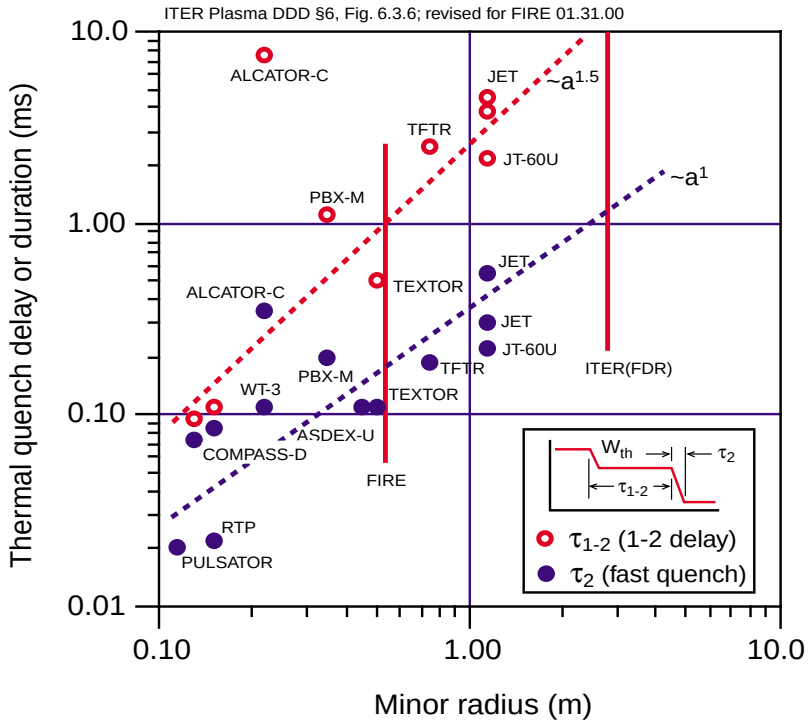

Fig. 1. Thermal quench data with application to FIRE
(empirical scaling, from *ITER Physics Basis*, Chapter 3)

The location of the thermal quench deposition is expected to be within the divertor channels. The 80-100% range reflects the possibility that up to ~20% W_{th} may be deposited on the divertor entrance baffle and/or the FW, since SOL widening of up to 10-x is sometimes seen in present experiments (3-x is more typical). The specific magnetic configuration aspects for FIRE of this type of broadening need to be checked.

Partitioning of the in-divertor energy between the inside and outside channels is relatively uncertain: however single-null plasma data typically show more energy to the inside channel. Figure 2 below, excerpted from the *ITER Physics Basis* Chapter 3, shows available data from DIII-D SN divertor plasmas. Total energy to the divertor normalized to pre-disruption thermal energy varies between ~20% and 100% (some data shows > 100%, presumably owing to experimental uncertainties). Energy ratio between inside (smaller R) and outside (larger R) channels is typically about 1, but high density disruptions and fast VDEs show an energy ratio up to ~3 (inboard energy ~3-x outboard energy). In some data, appreciable azimuthal asymmetries in target energy are also seen, and the lack of full azimuthal coverage leads to uncertainties about total energy.

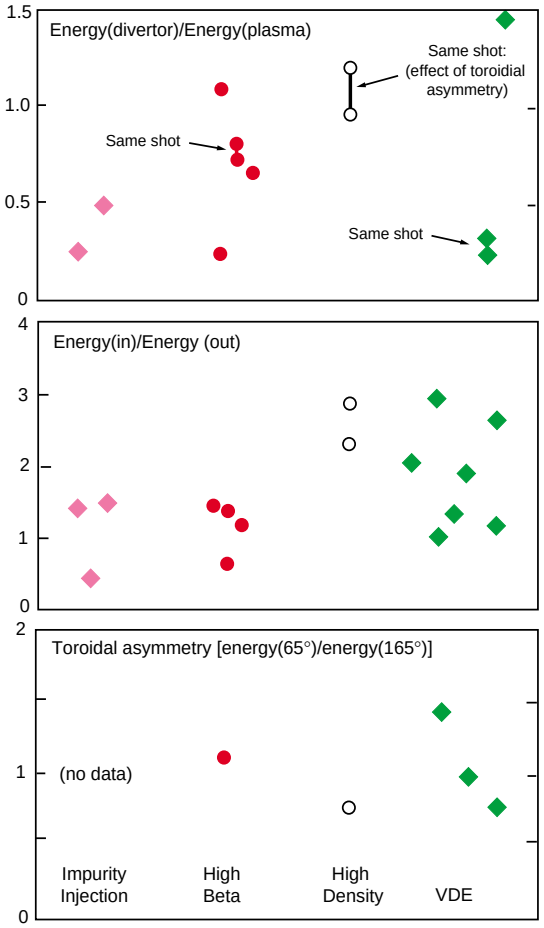

Fig. 2. Toroidal asymmetry ratio, inboard/outboard divertor target ratio and total energy accountability (referenced to plasma thermal energy) in various DIII-D single-null divertor disruptions and VDEs. The horizontal arrangement of the data within the four groups is for presentation purposes only and has no significance. Data and analysis by A. Hyatt, C. L. Lasnier, R. L. Lee, A. Kellman

Data on up/down energy balance during disruption was not available during the preparation of the *ITER Plasma DDD* and *Physics Basis*.

For a characteristic exposure time of 1 (10) ms, the thermal response of a material surface to incident energy received in a plasma environment makes a transition from surface heating and melting to vaporization and ionization at roughly 0.3 (1) MJ/m^2. The estimated magnitudes of the thermal-quench-phase divertor target deposition (active area ~2 m^2) and the current-quench-phase FW deposition (FW area ~70 m^2) in FIRE are respectively about 10 MJ/m^2 and 0.5 MJ/m^2. The corresponding surface responses will respectively be dominated by surface vaporization and ionization (divertor thermal quench, time scale ≤ 1 ms) and heating/melting (FW during current quench, time scale 2-10 ms, see below).

For the divertor, ionization and formation of a dense plasma-shielding layer near the material surfaces is predicted. This shielding layer and the ensuing onset of a 'hohlraum' effect will act to redistribute the incoming energy over a significant fraction of the total divertor channel surface (~10 m^2/channel). Prediction of the effects of vaporization and plasma ionization ('plasma shielding') must proceed primarily by modeling, since energy levels in present experiments are insufficient to explicitly test surface erosion in a plasma-shielding-dominated regime.

2. Current Quench Characteristics. Figure 3 shows a summary of current quench rate data (dI_p/dt) compiled by Fujisawa in 1997 to refine estimates of the expected current quench rate (duration) expected in ITER. The maximum current quench rate in the various tokamaks included in the database is found to scale linearly with pre-disruption average plasma current density $\langle j_{po} \rangle \cong I_{po}/(\kappa\pi a^2)$. The upper bound to the quench rate is commensurate with a mean current quench phase temperature of ~3 eV. This minimum temperature is in turn consistent with a simple radiative energy balance model in which impurity radiation from typical impurities (C) balances Ohmic heating power ($P_\Omega \sim \langle j_{po} \rangle$) during the current decay.

The estimated maximum FIRE quench rate at 6.5 MA is about 3000 MA/s. This corresponds to the 2 ms minimum quench duration given in Table 1 below. Note, however, that this estimate is based on extrapolation of data obtained in lower-field/lower-current-density tokamaks: direct data from Alcator C-Mod with current density comparable to FIRE does not exceed 1000 MA/s. This corresponds to 6 ms quench time in FIRE.

Note also that the empirical data suggests that minimum quench rate for FIRE may be as low as 10 MA/s, which implies up to a 600 ms quench time. Since the FIRE vertical instability growth rate is ~30 ms, appreciable vertical instability (a VDE) can be expected to develop during current quenches that are slower than ~100 MA/s.

The internal magnetic energy W_{mag} of a full-current FIRE plasma that is available for in-vacuum-vessel dissipation is approximately 35 MJ. Dissipation of W_{mag} (80-100%) in the current quench phase will be primarily by radiation to the FW, with a poloidal peaking factor ≤ 2. The resulting peak energy loading will be ~1 MJ/m^2. More localized deposition of the magnetic energy on the FW can also be expected if significant plasma motion (VDE) occurs during a slow (≥60 ms) current quench. Dynamic equilibrium evolution models that self-consistently include ex-plasma halo current must be used to predict this evolution and the resulting magnitude of such deposition for FIRE. The resulting energy loadings are presently relatively uncertain and model-sensitive, but may be as high as 20 MJ/m^2.

First wall energy levels of this magnitude are also possible (likely) if a 'hot plasma' VDE' occurs, wherein the initial plasma motion brings the still-hot (10 keV) plasma into contact with the FW before a thermal quench develops. Since plasma energy levels per unit surface area in present experiments are one to two orders of magnitude lower than energy levels in FIRE, present data on both cold-plasma and hot-plasma VDEs does not reflect the effects of localized energy loading and FW melting or vaporization.

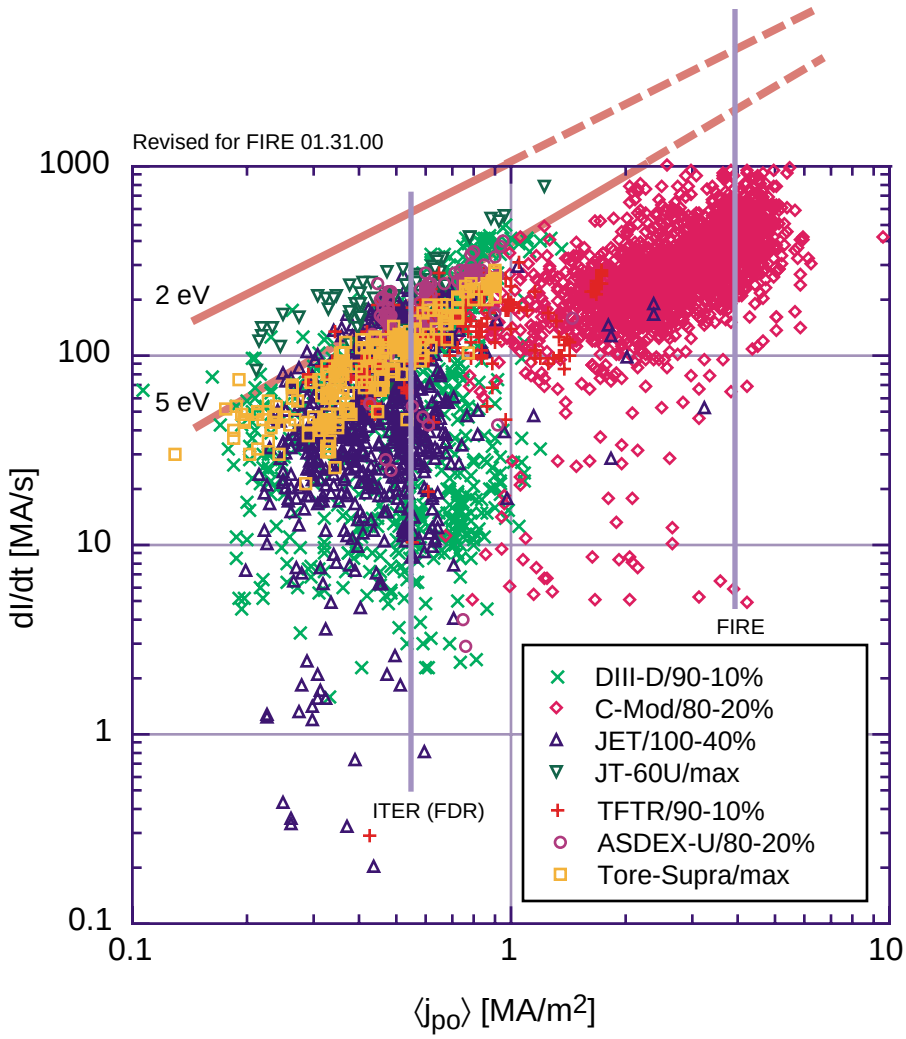

Fig. 3. Current quench database (various tokamaks), with contours of corresponding electron temperature superposed (calculated per Ohmic heating/radiation loss power balance model, see text)

3. Knock-on avalanche production of runaways

High current tokamaks such as FIRE may potentially be subject to the production of large numbers of runaway electrons during disruptions. The basic issue for runaway production in large tokamaks is that knock-on secondary electrons which can also run away lead to an exponential buildup of runaway current j_{RA} with growth rate γ_{RA} given to good accuracy by:

$$\frac{1}{j_{RA}}\frac{\partial j_{RA}}{\partial t} = \frac{1}{\tau_{RA}\ln\Lambda}\sqrt{\frac{\pi\gamma}{3(Z+5)}}\left(\frac{E}{E_c}-1\right)\left(1-\frac{E_c}{E}+\frac{4\pi(Z+1)^2}{3\gamma(Z+5)(E^2/E_c^2+4/\gamma^2-1)}\right)^{-1/2} \qquad (1)$$

Here E is toroidal electric field, $\gamma = (1 + 1.46\sqrt{r/R} + 1.72r/R)^{-1}$ is the neoclassical conductivity factor, $\ln\Lambda$ is the Coulomb logarithm, Z is effective charge of the main plasma, $\tau_{RA} = mc/eE_c$,

$$E_c = \frac{4\pi e^3 n_e}{mc^2}\ln\Lambda \cong 0.12 \cdot n_{e,20}\,[V/m] \qquad (2)$$

is the electric field necessary to balance the drag at the electron energy ~mc^2 and $n_{e,20}$ is electron density in units of 10^{20} m^{-3}. Growth rates projected using Eq.2 for typical FIRE parameters during the current decay phase — where densities are projected to be ~10 x 10^{20} m^{-3} and where $E >> E_c$ — are in the range $1000 \le \gamma_{RA}(s^{-1}) \le 10000$.

Equation (1) describes the growth rate given by a fit to Fokker-Planck theory that is valid in the region of positive growth rate. For fields smaller than the critical value given in Eq. (2), i.e., for $E < E_c$, there are no new runaways and existing runaways gradually slow down. This classical slowing down process is, however, relatively slow (~10 s) in a reactor tokamak and hence cannot be depended upon (without enhancement) to provide benign (without wall contact) runaway current dissipation.

Equation (2) implies that if runaways are to be unconditionally avoided during the current quench phase of a disruption, the electron density must be quite high,

$$n_{e,20} > \frac{10}{2\pi R}\frac{\Psi}{\tau}$$

where Ψ is the poloidal flux available during the current quench (≈10 Wb in FIRE), and τ is the current quench time. For the 6-60 ms range of disruption-initiated current quench times expected in FIRE an after-disruption density $n_{e,20} \ge 130–1300$ is required for unconditional runaway avoidance. It is very unlikely that densities in this range will be occur naturally during disruptions. If densities of this magnitude are obtainable at all, the most likely means for attaining them appears to be injection of massive amounts (~0.1 kg) of deuterium in the form of multiple solid pellets or as a liquid jet.

While FIRE is not exempt from runaway avalanching during disruptions, the overall avalanche gain factor, $\exp(\gamma_{RA}t)$ is only (!) about 10^6. This estimate follows from the analysis developed in by Rosenbluth and Putvinski (*Theory for Avalanche of Runaway*

Electrons in Tokamaks, Nuclear Fusion **37** (1997) 1355), wherein the number of e-folds ($\gamma_{RA}t$) is estimated to be $I_p/(I_A \ln\Lambda) \cong 2.5\ I_p(MA)$. Here $I_A = mc^3/e \cong 0.02$ MA is the Alfvén current. For FIRE, the estimate avalanche gain is $\exp(15) \cong 10^6$.

This relatively low gain is to be contrasted for the much higher gain factor estimated for larger size/current tokamaks such as ITER FDR (21 MA), where the gain is ~$\exp(50) = 3 \times 10^{19}$. At this gain, even a minute initial 'seed' population of superthermal electrons — e.g., fast electrons from Compton scattering of first-wall-activation gammas — is sufficient to yield nearly complete conversion of the initial plasma current to 10 MeV runaway current. Studies for ITER show up to 15 MA runaway current relative to 21 MA plasma current.

In FIRE, the lower avalanche gain makes multiplication of such low-level seed sources to appreciable levels unlikely. For avalanching to be significant in producing runaways in FIRE, the initial seed source must be > ~1 A. This high superthermal population is not expected in a normal (thermal) FIRE DT burning plasma. However, there could be a possibility that high-Z pellets (killer pellets) injected into such a plasma for plasma thermal energy dissipation (fast shutdown) may generate localized runaways in the cold plasma pellet ablation 'wake' that could then avalanche to appreciable levels (≥ 0.1 MA). If so, the ensuing FIRE current quench or VDE might acquire an appreciable runaway content, and multi-MA runaway current could arise.

Runaway production by this pellet injection mechanism has been observed in DIII-D. In DIII-D, avalanche gain is small, so the effect of these runaways is seen mainly as enhanced hard X-ray emission when the pellet-created electrons eventually reach the limiter or first wall. Exactly what will happen to pellet-created runaways in FIRE with avalanching needs to be examined further.

4. Vertical Disruptions, VDEs and Halo Current. Vertical instability plays an important role in the current quench phase of disruptions in vertically-elongated tokamaks, and the resulting generation of poloidal current flow ('in-vessel halo currents') in electrically-conducting in-vessel components gives rise to significant local and global forces on the in-vessel and torus vessel systems of such tokamaks. In a reactor-scale experiment such as ITER, the estimated maximum magnitudes of the in-vessel current and total vertical force are respectively about 8 MA and 150 MN. In FIRE, the respective estimates are about 2.5 MA and 25 MN. In either device, accommodating this current flow and the resulting electromagnetic (EM) forces becomes an important design consideration.

Vertical instability: causes and consequences. Since elongated plasmas are vertically unstable, a sufficiently large and fast change in plasma parameters (I_p, β, l_i, and/or elongation) can cause a loss of vertical position control, leading to an uncontrolled upward or downward displacement of the plasma column and plasma contact with structures at the top or bottom of the chamber/first wall/divertor. Such a scenario is a common outcome of a major disruption in a elongated-cross-section tokamak with a single-null divertor. Figure 4shows an example of a typical elongated-plasma disruption in Alcator C-Mod. Vertically-unstable disruptions with similar characteristics are observed in all presently-operating elongated-cross-section divertor tokamaks, including ASDEX-Upgrade, COMPASS-D, DIII-D, JET and JT-60U.

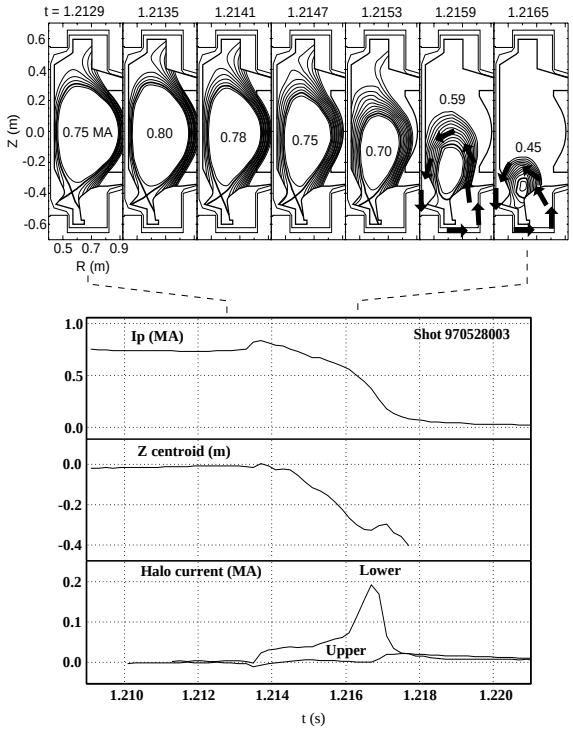

Fig. 4. (a) Magnetic flux reconstructions at 0.6-ms intervals during a disruption and subsequent vertical displacement in Alcator C-Mod. Arrows show the poloidal projection of halo current flow. The halo circuit in the plasma scrape-off actually follows a helical path. (b) Plasma current, vertical motion, and in-vessel halo currents in the upper and lower portions of the vacuum vessel wall.

The disruption process begins with a thermal quench, in which most of the plasma thermal energy is rapidly lost through radiation and/or conduction to the divertor strike points. The fast changes in β, l_i, etc. which accompany the thermal quench lead to a loss of vertical

position control. In the ensuing vertical displacement phase of the disruption, the plasma elongates (owing to the current profile broadening and decrease in l_i that follows the onset of the thermal quench) and moves rapidly downwards, and eventually comes into full poloidal contact with the lower portion of the plasma-facing first-wall and divertor entrance baffle structures. Significant poloidal current flow in these structures occurs in this displacement termination phase. Peak poloidal currents in the example shown are about 200 kA, or about 25% of the initial before-disruption plasma current I_{p0}. This peak normalized current magnitude is both representative of what is typically seen in present tokamaks and what extrapolation of present halo current data predicts as the typical halo current magnitude for FIRE.

The magnetic energy stored in the poloidal field of the plasma current decays on a slower time scale than that of the vertical motion, and usually the magnetic energy is not dissipated until the plasma contacts and terminates at the top or bottom of the chamber. Note in Fig. 4 that more than one-half of the initial plasma current still remains in the last frame, where the plasma core (region of closed flux surfaces) is localized almost within the divertor entrance and where most of the plasma current flow is now in the wall-intersecting halo-current scrape-off-layer which surrounds the core.

In addition to the preceding disruption-produced VDE scenario, it is also possible to lose vertical position control without a disruption thermal quench. Faults in the vertical position feedback control system (power supply failures, sensor failures, power supply voltage/current limitations), running plasmas with excessive elongations, or even large ELMs can result in initiation of an uncontrolled vertical displacement. The main difference between this type of vertical displacement event (VDE) and a thermal-quench-initiated 'vertical disruption' is that the thermal quench and current quench occur simultaneously. This type of VDE can be termed a 'hot-plasma' VDE to distinguish it from a 'cold plasma' VDE or vertical disruption in which thermal energy loss is essentially complete before appreciable vertical motion develops. Since modeling predicts that higher plasma edge temperature will lead to higher halo current fractions, hot plasma VDEs are expected to have higher halo current fractions (see discussion below) and halo current EM loadings. Hot-plasma VDEs in a reactor plasma will also have plasma-wall interaction consequences (impurity release and wall melting and vaporization) that are not present or appreciable in hot-plasma VDEs in present experiments.

The direction of vertical disruptions in present single-null tokamaks is typically but not universally downwards, towards the divertor. Upwards (away from the divertor) displacements after disruption are sometimes observed, particularly in disruptions in which full current profile broadening ($l_i \rightarrow \sim 0.5$) is not obtained. Simulations of the initial dynamics of disruptions with axisymmetric equilibrium models (e.g. TSC or DINA) show that the direction of initial motion is determined by the competition of the equilibrium-modifying effects of current profile broadening and pressure loss with the separate effect of the induced toroidal eddy currents in in-vessel and vessel structures that arise from the initial current decay. For loss-of-control VDEs, the initial direction is usually random.

Vertical control loss in SN plasmas after disruption is not inevitable. In rare instances (typically with lower elongation plasmas and very fast current quenches), the after-disruption plasma in Alcator C-Mod remains in approximate vertical equilibrium and the plasma motion is radially inward. In these passively-stable cases, halo currents appear mainly in the inboard wall. A similar passive 'neutral-point' behavior is obtained — with careful selection of the initial pre-disruption vertical position — for more-elongated single-null plasmas in JT-60U, and with optimization of the vertical position control algorithm, active control of the plasma position after a thermal quench can be maintained for a certain range of plasma configurations and current decay rates. In these vertically-stabilized disruptions, the halo currents seen in the lower portion of the vessel in vertically unstable disruptions are absent. However, whether inner-wall halo currents are present is not known (no diagnostics).

Plasma operation near the neutral point with a single null or in a double null and with adequate vertical position control is a potential means for VDE and halo current avoidance in reactor tokamaks and in FIRE. However, predicting the degree to which active control can be maintained in FIRE after a DN disruption and what the effect of residual asymmetries and plasma control noise will be are still open issues. So the frequency of after-disruption VDEs in FIRE with a DN configuration is uncertain.

Halo currents: During a vertical disruption or a VDE, both the plasma current and the cross-sectional area (which encloses toroidal flux) decay to zero. Both decays generate an electric field which can drive current flow along the helical field lines in the scrape-off region of the plasma. This so-called 'halo' current was first explicitly observed on JET and DIII-D. Indirect but compelling evidence for the existence of halo currents was also obtained for vertically-unstable disruptions in PBX-M and halo-currents are now understood to have

been responsible for what at the time were inexplicable incidents of mechanical or attachment-heating damage to in-vessel components in early tokamak experiments.

The halo current flowing helically on wall-intersecting plasma flux surfaces makes a complete circuit by flowing from the strike points at one end of the open SOL field lines, through the conducting first wall structures, and out onto the other end of the SOL field lines. The poloidal projection of the halo current flow is shown in the last frames of Fig. 4. Measurements in Alcator C-Mod show that for downward-going disruptions, halo currents flow only in the bottom portion of the chamber, as shown in Fig. 4, and vice versa for upward-going disruptions. In the rare instances when a disrupting plasma remains at the midplane (usually for near-circular plasmas), halo currents are observed at the vessel midplane. Figure 4 shows that the time of maximum halo current occurs around the time of maximum current quench rate, and that the plasma is still carrying about 60% of the initial plasma current, even though it has shrunk dramatically in size. The value of q_{edge} at or near the last closed flux surface is low and is typically (within the approximations inherent in the magnetic reconstructions shown in Fig. 4) equal or less than unity. Similar localization of the terminating plasma and near-unity values of the core safety factor obtained with a full Grad-Shafranov equilibrium reconstruction are found for DIII-D and JT-60U VDEs.

The poloidal halo current flowing in the wall, when crossed with the toroidal magnetic field, gives rise to additional structural forces above and beyond the well-understood toroidal or saddle eddy current forces induced during disruptions. Experimental measurements and numerical simulations on ASDEX-U and DIII-D have shown that the forces associated with halo currents are a major contributor to the vertical force acting on the torus vessel during a disruption. Representative force data from ASDEX-U are shown in Fig. 5. Estimates of the effective radial width Δr_{eff} for the in-vessel halo current flow path derived from such data show that the effective width is comparable to the initial plasma minor radius. These width estimates confirm the localization and estimated width at maximum displacement derived from magnetic reconstructions of the type shown in Fig. 4.

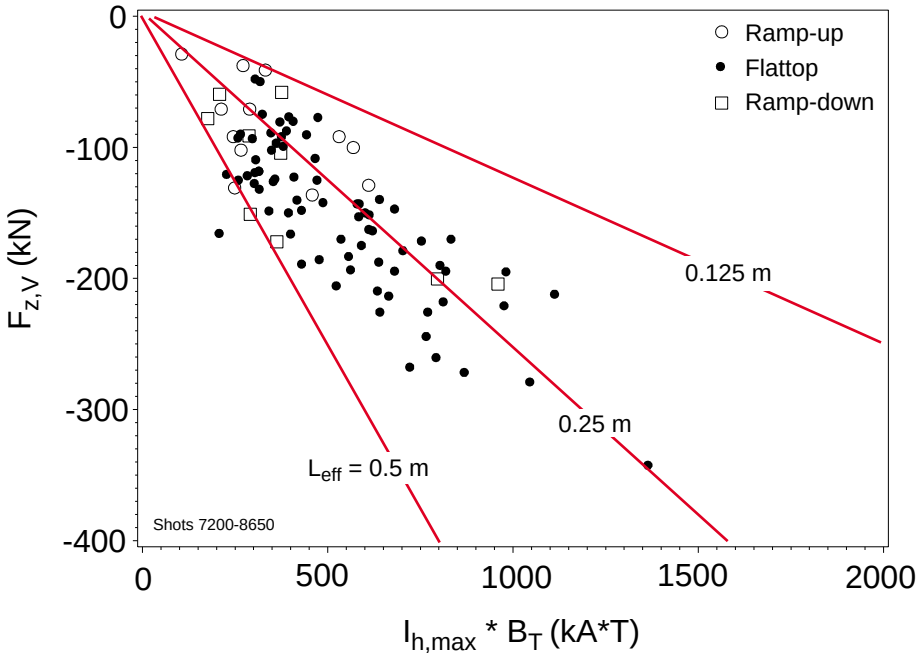

Fig. 5. Measured vertical disruption forces in ASDEX-U compared with the product of maximum halo current (measured) and toroidal field. The mean slope of the data implies an effective in-vessel halo current flow length of about 0.4 m (~$0.8a_o$). The toroidal conductivity of nearby in-vessel components is negligible, so in this case, halo current provides the entire vertical stabilizing force on the plasma.

Vertical forces: The global magnitude of the total vertical force produced during a vertical disruption or a VDE can be estimated on a very simple basis from the plasma destabilizing force

$$F_{Z,max} \approx 0.7\, I_0\, \Delta Z_{max}\, \partial B_{r,eq}(\Delta Z_{max})/\partial Z \qquad (3)$$

where I_0 is the pre-disruption or pre-VDE plasma current, $\partial B_{r,eq}/\partial Z$ is the radial equilibrium field gradient evaluated at the location ΔZ_{max} of maximum plasma column displacement (typically near the top or bottom of the in-vessel structure) and the numerical factor of ~0.7 is chosen to reflect the experimental observation that the plasma current at maximum displacement is typically about two-thirds of the initial current. Applying Eq. (3) for typical ITER parameters with I_{p0} = 21 MA gives a maximum vertical force of about 150 MN (15,000 tonnes). Since the plasma must be in force balance, the total vertical force developed on the in-vessel and vessel systems by toroidal and poloidal eddy currents and by in-vessel halo currents cannot exceed this value. Comparison of the force estimated by Eq. (3) with either mechanical measurements of the actual vertical force or estimates of the $I_{h,max}B_T\Delta r_{eff}$ force derived from in-vessel halo current measurements and knowledge

of the halo current flow geometry confirms that the expected in-vessel/vessel vertical forces are obtained and are in good agreement with corresponding plasma destabilizing force.

While estimates of the maximum vertical force derived from Eq. (3) can provide a good basis for the design of the vessel support system in future tokamaks, in order to specify the engineering design constraints on the first wall for reactor tokamaks, the magnitude and in-vessel distribution of the halo current needs to be specified. To this end, the ITER Expert Group on Disruptions, Plasma Control and MHD compiled a database of disruption information, including halo current measurements, from a number of present-day tokamaks. As shown in Fig. 6, for ITER- and FIRE-relevant elongations in the range of 1.5–2.0, the peak halo current ($I_{h,max}$) seen in present tokamaks can range between about 1% and 50% of the pre-disruption plasma current (I_{p0}).

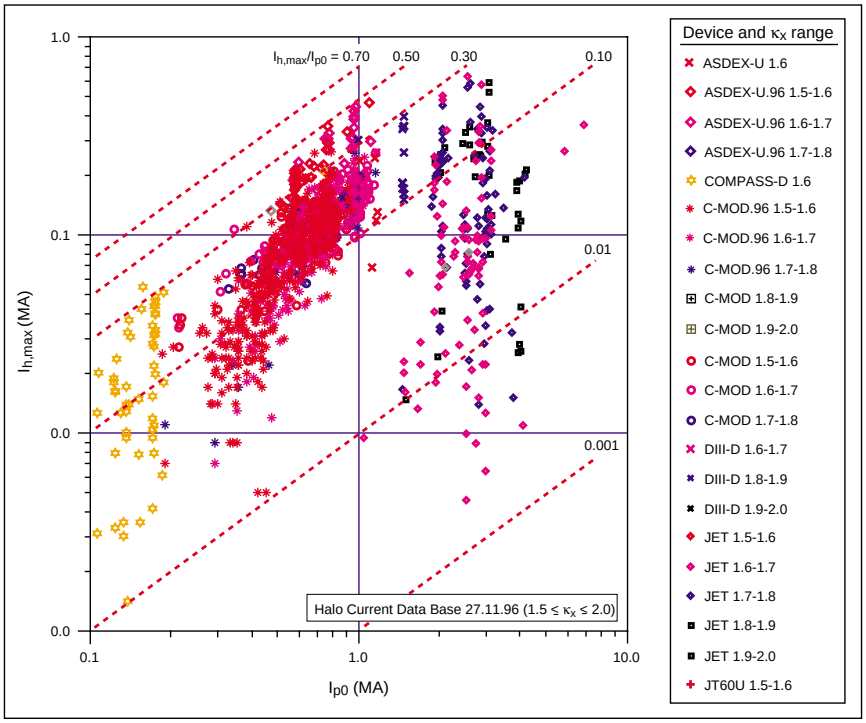

Fig. 6. Peak total halo current ($I_{h,max}$) versus pre-disruption plasma current (I_{p0}) for disruptions in various elongated tokamaks. The data is for plasmas with vertical elongation $1.5 \leq \kappa_X \leq 2.0$, where κ_X is the elongation at the separatrix.

The large amount of scatter in the maximum halo current data within a single experiment and within the database as a whole suggests that there are one or more underlying 'hidden variables' in the data set. However, systematic analysis of the database in terms of the elongation and/or q_{95} sensitivity has failed to show any clear systematic multi-machine

dependence on these parameters or on plasma size of current or on after-disruption 'cold-plasma' VDEs versus comparable loss-of-control 'hot-plasma' VDEs. While there are clearly discernible systematic I/q_{95} and/or I_p/B_T dependencies in the Alcator C-Mod data these same dependencies are not as clearly evident in the remainder of the database. For the database contributions in which a significant range of elongations is present there is also no explicit elongation (κ_x) dependence for normalized halo current magnitude except for obvious cases where the elongation is insufficient to result in vertical instability. Selecting $\kappa_x \geq 1.5$ removes these vertically-stable cases from the database.

The higher maximum halo current fraction observed in ASDEX-U (up to 50% as contrasted with 30-40% in other experiments) stands out in the overall database and is likely the result of the lack of appreciable vertical stabilizing effect from induced toroidal currents (the saddle-connected vertical stabilizing structure in ASDEX-U is ineffective for vertically-displaced plasmas). If this aspect of the ASDEX-U data is taken into account, the maximum normalized halo current fraction that can be inferred from Fig. 6 is about 40%, and the majority of the data lies below 30%. The upper bound of the halo current fraction set for ITER design is 40% (8 MA for I_{p0} = 21 MA). The same recommendation for FIRE translates to 2.6 MA. However, since the FIRE passive stabilizing system may have characteristics similar to ASDEX-U, a higher halo current fraction of 50% (3.2 MA) may apply.

The measurements in Fig. 6 have been assembled from tokamaks of many different minor radii (0.16 m to 1.25 m). At the present time, understanding of the variance in the data is not yet adequate to determine whether or not halo current fraction depends on machine size, but the JET and JT-60U data in Fig. 6 and more-recently-reported measurements of halo current magnitude in JET and further magnitude data from JT-60U increasingly suggest that larger-R machines have a normalized maximum halo current fraction ($I_{h,max}/I_{p0}$) that does not exceed about 25%. But this possible 'large tokamak' scaling benefit will not apply to FIRE, and there is no evidence of a favorable 'high-field' scaling (eg., C-Mod and COMPASS-D data are quite similar).

Halo current distribution, toroidal asymmetries, and lateral loads: While the upper bound on the expected collective vertical force on in-vessel and vessel systems can (subject to some uncertainty about the magnitude of the plasma current at maximum displacement) be estimated from the elementary considerations embodied in Eq. (3), and the expected magnitude of the maximum expected halo current can be derived from empirical analysis of

the halo current database, evaluation of local forces and stresses in the vessel chamber/first wall/divertor requires knowledge of the toroidal and poloidal distribution of in-vessel halo currents. Here in-vessel measurements and magnetic reconstructions in a number of tokamaks have shown that (1) the poloidal width of the halo region is relatively narrow ($0.2a_o$–$0.3a_o$) and remains approximately constant as the vertical displacement proceeds and the closed-flux-surface plasma core radius decreases, and (2) there are significant toroidal asymmetries present. These asymmetries have important design implications, since they result in toroidal peaking of the in-vessel halo current flow and $\mathbf{j} \times \mathbf{B}$ force, and as elementary analysis shows, a net radially-directed sideways or lateral loading on the in-vessel/vessel system. Lateral displacement of the JET vacuum vessel has been observed in certain VDEs. Lateral loadings are an important design issue for reactor tokamaks, since most previously-proposed solutions for support of in-vessel and vessel systems have not explicitly addressed the possibility of such loads. The mechanical problem is significant in both present and future tokamaks: the lateral loads inferred for a 3.5-MA JET VDE are ~2 MN and a simple I_p*B_T*R scaling of this value to FIRE yields lateral loads of ~8 MN.

Measurements of the toroidal symmetry of halo currents in the six tokamaks contributing to the IDDB give typical toroidal peaking factors (TPF, defined as ratio of maximum halo current density to toroidally-averaged halo current density) in the range of 1.2–2, although there are also some data with TPF greater than 3. An example of the toroidal distribution and temporal behavior of halo currents in a typical Alcator C-Mod vertical disruption is shown in Figs. 7a and 7b. A basic n = 1 structure of the toroidal distribution is clearly seen. There is also evidence of higher-n modes and for dynamic variation of the fine structure of the current distribution within the time-scale of the halo current pulse. Furthermore, in C-Mod this structure is usually seen to rotate toroidally at frequencies of order 1 kHz. This rotation rules out first-wall non-uniformities as the cause of the asymmetry.

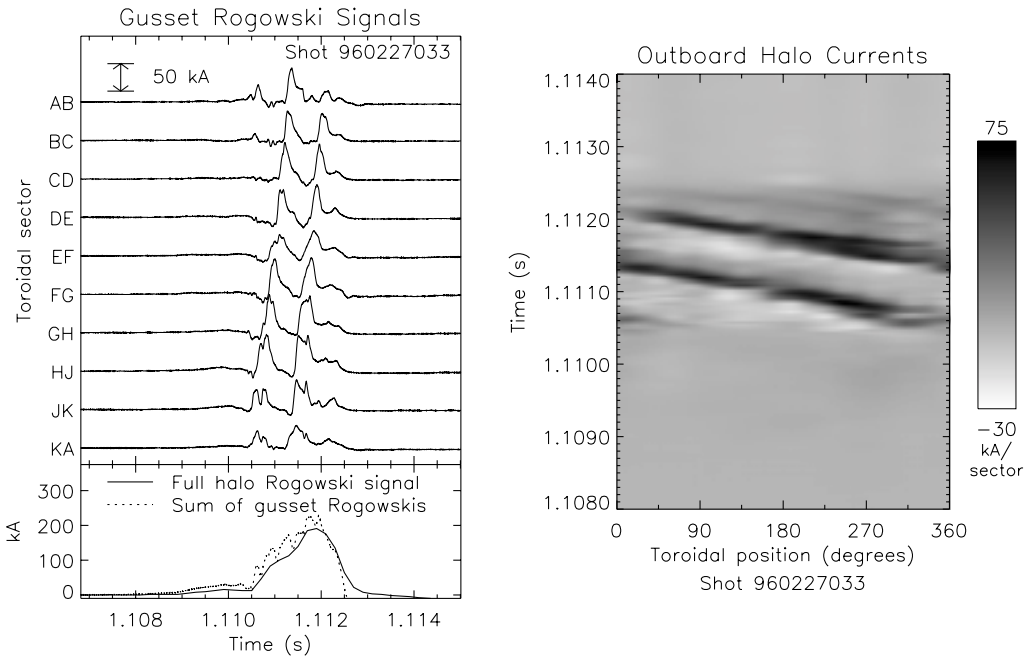

Fig. 7a and 7b. Halo current density measured at 10 toroidal locations around the Alcator C-Mod divertor: (a) A relatively peaked `filament' of halo current is seen to rotate twice around the torus. (b) The same data plotted in a different manner, showing the predominantly n = 1 structure of the toroidal asymmetry.

Detailed measurements of the spatial structure in C-Mod show that the halo current flow in the vessel structure is purely poloidal. This implies that the wall-intersecting field lines carrying the halo current must make an integer number of toroidal transits in going from the entrance strike point to the exit strike point (typically one toroidal transit in C-Mod), and hence there may be a resonance condition for halo current flow which involves the field line helicity. Depending upon the geometry of contact, this also implies that q_{edge} has to be between 1 and 2. This is consistent with the previous observation derived from magnetic reconstruction concerning the low plasma core safety factor in the last frame of Fig. 4.

Rotation of the halo current asymmetry is not observed on all machines, or even on all disruptions in a single machine. In general, non-rotating asymmetries are observed in larger machines. The observation of low (near-unity) edge-q in the final maximum-displacement phase of the current decay is, however universal, as is the presence of some degree of an n = 1 structure. For moderate asymmetries, $1 \leq TPF \leq 2$, the resulting azimuthal dependence of the toroidal distribution can be described to a reasonable approximation as $j \sim j_o(1 + \delta \sin\phi_{tor})$ where ϕ_{tor} is the toroidal coordinate. For cases with TPF ≥ ~2, the n = 1 structure is increasingly modified by higher-n harmonics that reflect localization of

the in-vessel halo current in a relatively small fraction of the full torus circumference. The resulting distribution of halo current approaches a toroidally-localized peak or 'filament' with low or zero current elsewhere. Figure 8 shows an example of a high-TPF halo current distribution obtained in an Alcator C-Mod disruption at times near the halo current magnitude peak. The calculated TPF for the three times varies between 2.5 and 3.8 and the halo current is localized within approximately three of the ten equally-spaced divertor support structure modules. While detailed evidence for the exact degree of toroidal localization in present tokamaks is somewhat limited owing to the finite toroidal number and resolution of in-vessel halo current measurements, the possibility of a relatively-high toroidal localization of in-vessel halo current in reactor tokamak VDEs is a design aspect that must be taken into consideration.

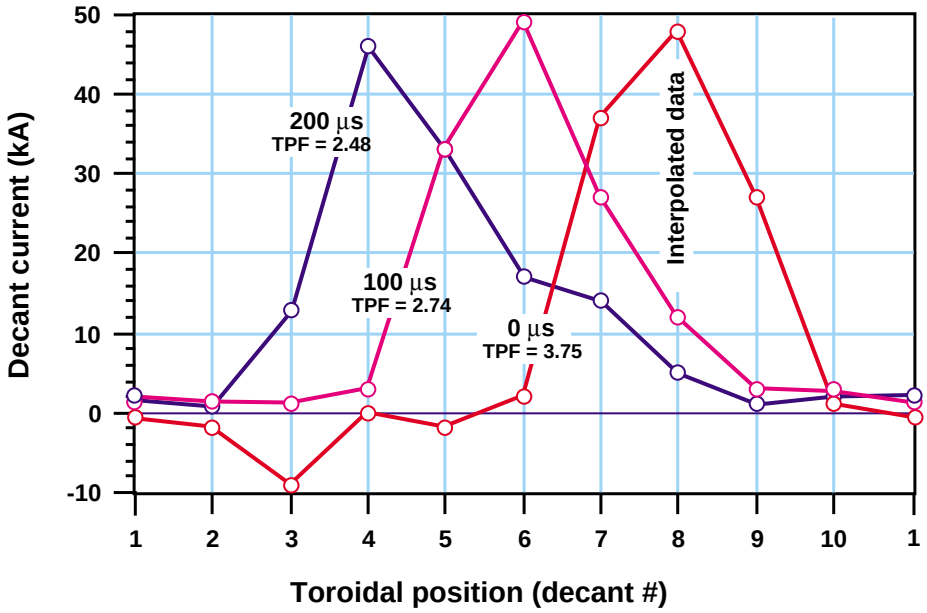

Fig. 8. Halo currents in the Alcator C-Mod divertor structure (ten electrically-isolated decants) at three 100-ms intervals near the time of maximum halo current. Halo current at a given time is largely localized within 3 to 4 of the 10 equally-spaced divertor support modules. The TPF varies between 2.5 and 3.8. The distribution rotates toroidally at a frequency of 1.4 kHz

Toroidal peaking factor: Information on the toroidal peaking of halo currents in a number of tokamaks has been assembled as part of the ITER Disruption Database as shown in Fig. 8. It is apparent that the higher peaking factors tend to be seen only at lower normalized halo currents. A hyperbolic relationship can be used to define a bounding curve, which can then be used for engineering design guidance. The curves shown in the Figure for

$(I_{h,max}/I_{p0})$*TPF = 0.75 and $(I_{h,max}/I_{p0})$*TPF = 0.50 have been recommended as 'worst-case' and 'typical maximum' bounds for ITER halo current magnitude.

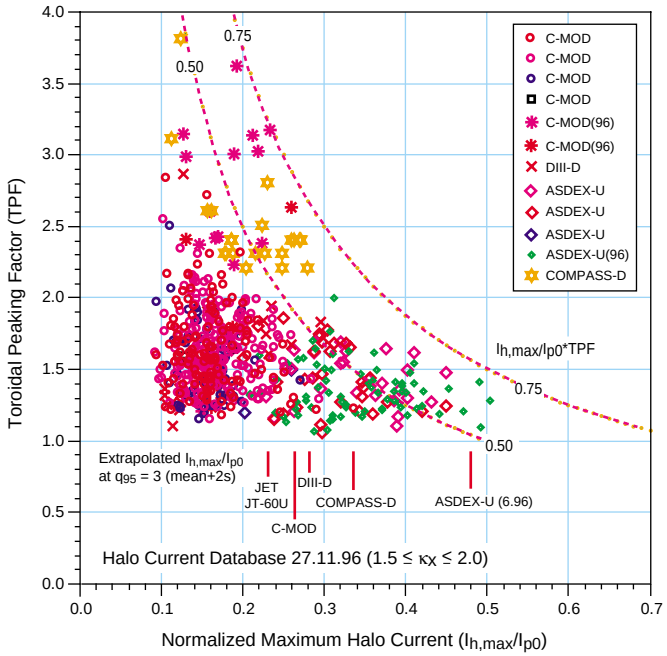

Fig. 9. Toroidal peaking of halo currents in tokamaks, for plasmas with $1.5 \leq \kappa_X \leq 2$. High peaking factors occur only at low halo current fraction. The hyperbolic curves show limiting bounds for the data. The bounds in the various tokamaks on the normalized maximum halo current at $q_{95} = 3$ derived from the data in Fig. 3 are also shown.

There is some theoretical justification for this hyperbolic bound. This justification derives from semi-empirical models derived by Pomphery that explain the n = 1 character of the in-vessel current asymmetry on the basis of the interaction of an n = 1, m = 1 helically-deformed plasma column with an axisymmetric conducting shell. Toroidally non-uniform contact of the halo region of the deformed plasma gives rise to the n = 1 variation of the shell halo current and variation in the degree of contact during the VDE evolution gives rise to an inverse correlation of halo current magnitude and TPF that is qualitatively similar to the bounds of the data in Fig. 9. The addition of higher order n/m modes to the deformation could explain both the toroidal localization that occurs at higher TPF and the dynamic fine structures that are visible in the data in Fig. 7.

A similar explanation of the n = 1 character of the asymmetry and an estimate of the lateral vessel force measured in JET can be obtained for a plasma that is tilted and/or radially displaced with respect to the JET vessel shell. Measurements of the axial and radial position of the plasma cross-section in JET at various toroidal locations during toroidally-

asymmetric VDEs confirm the existence of a non-rotating tilted and/or deformed plasma in cases where appreciable sideways displacement of the vessel system is observed. The measured maximum tilt displacements (difference in plasma axis height on opposite sides of the torus) are about ±0.15 m, or ±15% of the nominal minor radius. There is also an ~0.02 m off-center shift of the plasma torus axis relative to the vessel torus axis. There are also indications that higher-n or m plasma deformations are present. Finally, analysis of the electromechanical loading expected for this type of tilted plasma and the measured mechanical response of the torus and torus support system are found to be in reasonably good agreement.

The development of an n = 1 m = 1 'external' kink instability at the q = 1 termination phase of a vertical disruption or VDE is an obvious candidate for explanation of the toroidal asymmetries seen in present experiments, and modeling of such a deformed plasma with a three-dimensional MHD equilibrium code would provide a quantitative basis for both interpretation of present plasma displacement and halo current data and for the prediction of halo current asymmetries and vessel forces in future tokamaks. However, clear measurements of a helically-deformed or tilted plasma in experiments other than JET remain to be obtained, and modeling of a helically-deformed plasma with halo currents in self-consistent equilibrium with an axisymmetric conducting shell remains as a future challenge to the MHD equilibrium and stability modeling community.

Extrapolation to FIRE: The halo current and VDE design basis recommended for FIRE are maximum vertical and lateral forces of 25 MN and 8 MN respectively, $I_{h,max}/I_{p0} \leq 0.4$ (≤ 0.25 typical), $1.2 \leq TPF \leq 4$ and $(I_{h,max}/I_{p0})(TPF) \leq 0.75$ (≤ 0.50 typical). Furthermore, pending final design of the FIRE passive stabilizing structure(s), $I_{h,max}/I_{p0} = 0.5$ needs to be examined as a possible design condition.

These guidelines are set to define worst-case limits, and there is a possibility that they can be relaxed in the future if improved understanding of the degree to which disruptions and VDEs in FIRE (with a DN configuration) will lead to a distribution of loading conditions rather than worst-case limits. Better specification of such 'statistical' aspects of disruption and VDE loading may become relevant to future regulatory assessments of DT-burning and reactor tokamak functional and structural integrity in normal and 'off-normal' operation conditions.

The question of the possible tokamak size (major radius) scaling of the maximum halo current fraction is one of the principal remaining uncertainties about halo current magnitude. Fig. 10 shows recent halo current data from JET and JT-60U superposed on the data presented in Fig. 9. There is some evidence in the superposition for a weak favorable scaling of peak halo current magnitude and $I_{h,max}/I_{p0}$ with increasing tokamak dimension. But the data from all machines — both small and large— is quite scattered and the reasons for why there is such a wide range of maximum halo current and asymmetry for a given equilibrium are not well understood, nor is the possible dependence of such parameters on vessel/divertor structural geometry in the contact region and other machine-specific parameters. In this latter regard, in future halo current data taking, it will be important to have as extensive an array of in-vessel halo current diagnostics as possible (full poloidal and toroidal coverage of first-wall currents in existing experiments is limited to at least some degree and in-vessel component halo current flow paths are not always fully instrumented) and to attempt to make more definitive correlations among non-axisymmetric plasma displacement measurements, halo current asymmetries and in-situ measurements of forces and/or stresses in in-vessel components. This recommendation extends to FIRE itself: a comprehensive set of plasma configuration, in-vessel halo current and in-vessel and vessel structural response diagnostics is recommended.

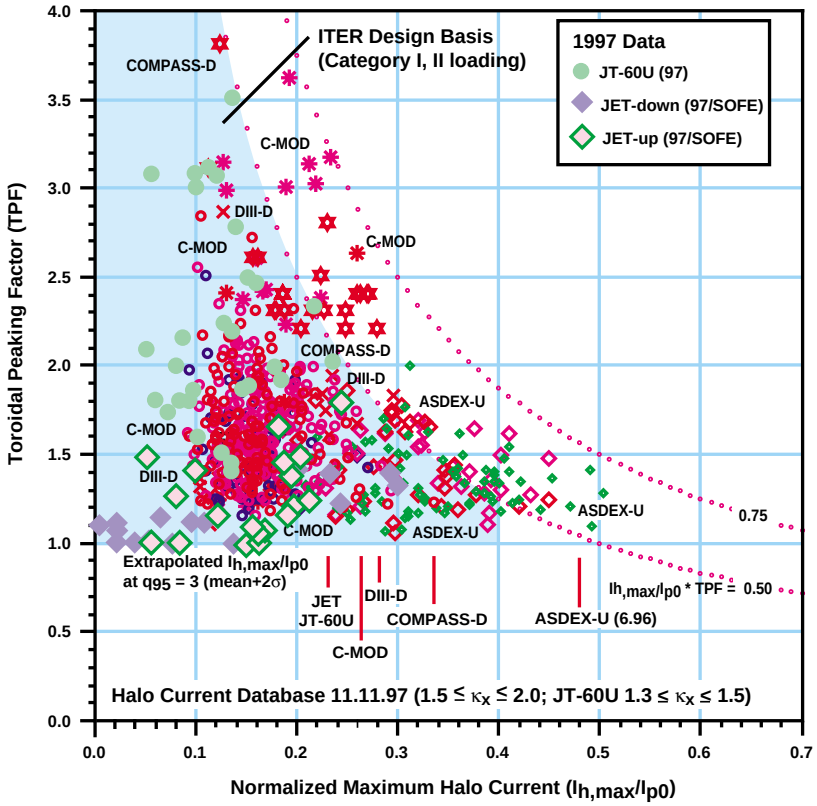

Fig. 9. Halo current database, data selected for $1.6 \leq \kappa_X \leq 2.0$. Recent data reported by JET and JT-60U is added to the 1996 data. The shaded $I_{h,max}/I_{p0}$ vs. TPF domain shows the loading condition envelope established for ITER in-vessel and vessel component design for so-called Category I and II loading conditions (routine/normally-expected events)